

Batteries

 International Edition: DOI: 10.1002/anie.201804114
 German Edition: DOI: 10.1002/ange.201804114

A Perovskite Electrolyte That Is Stable in Moist Air for Lithium-Ion Batteries

Yutao Li, Henghui Xu, Po-Hsiu Chien, Nan Wu, Sen Xin, Leigang Xue, Kyusung Park, Yan-Yan Hu, and John B. Goodenough*

Abstract: Solid-oxide Li^+ electrolytes of a rechargeable cell are generally sensitive to moisture in the air as H^+ exchanges for the mobile Li^+ of the electrolyte and forms insulating surface phases at the electrolyte interfaces and in the grain boundaries of a polycrystalline membrane. These surface phases dominate the total interfacial resistance of a conventional rechargeable cell with a solid–electrolyte separator. We report a new perovskite Li^+ solid electrolyte, $\text{Li}_{0.38}\text{Sr}_{0.44}\text{Ta}_{0.7}\text{Hf}_{0.3}\text{O}_{2.95}\text{F}_{0.05}$, with a lithium-ion conductivity of $\sigma_{\text{Li}} = 4.8 \times 10^{-4} \text{ S cm}^{-1}$ at 25°C that does not react with water having $3 \leq \text{pH} \leq 14$. The solid electrolyte with a thin Li^+ -conducting polymer on its surface to prevent reduction of Ta^{5+} is wet by metallic lithium and provides low-impedance dendrite-free plating/stripping of a lithium anode. It is also stable upon contact with a composite polymer cathode. With this solid electrolyte, we demonstrate excellent cycling performance of an all-solid-state $\text{Li}/\text{LiFePO}_4$ cell, a Li-S cell with a polymer-gel cathode, and a supercapacitor.

Replacement of the flammable organic liquid electrolyte of a Li-ion battery by a non-flammable solid Li^+ electrolyte from/to which low-impedance dendrite-free plating/stripping of a metallic-lithium anode can occur over a long cycle life is a high-priority technical target.^[1] Dendrite-free plating/stripping of a lithium anode over a long cycle life requires not only wetting of the solid electrolyte by metallic lithium,^[2] but also an electric energy gap for the solid electrolyte of $E_g > 5 \text{ eV}$ that has the bottom of its conduction band above the Fermi level of metallic lithium.^[3] High rates of charge/discharge require a low impedance for plating/stripping across the electrode/electrolyte interface as well as an ionic conductivity of $\sigma_i > 5 \times 10^{-3} \text{ S cm}^{-1}$ at the operating temperature T_{op} of the cell.^[4] Solid Li^+ electrolytes previously reported are mostly moisture-sensitive and plagued by the formation of insulating

surface layers on grain boundaries and at the anode/electrolyte interface that reduce the σ_i value of a polycrystalline electrolyte membrane.^[5] Moreover, interfacial degradation also prevents wetting of the solid electrolyte by lithium and introduces a large interfacial resistance that increases with cycling.^[6] Herein, we report a new oxo-perovskite Li^+ electrolyte, $\text{Li}_{0.38}\text{Sr}_{0.44}\text{Ta}_{0.7}\text{Hf}_{0.3}\text{O}_{2.95}\text{F}_{0.05}$, that provides low-impedance plating/stripping of a lithium-metal anode over a long cycle life if a thin Li^+ -conducting polymer coats the surface contacting the anode; this coat suppresses the reduction of Ta^{5+} . Fluorine doping helps reduce the interfacial resistance of the battery. The solid electrolyte is moisture-tolerant at $3 \leq \text{pH} \leq 14$ and also retains a low-impedance interface with a composite cathode. Full-cell assembly is facile, and low-cost full cells with a long cycle life are demonstrated.



$\text{Li}_{0.38}\text{Sr}_{0.44}\text{Ta}_{0.75-x}\text{Hf}_{0.25+x}\text{O}_{3-x}\text{F}_x$ ($0 \leq x \leq 0.1$) samples prepared by regular high-temperature sintering have a cubic perovskite structure (Figure 1a; see also the Supporting Information, Figure S1 a); only a very small amount of the SrTa_2O_6 secondary phase exists. The lattice parameter of $\text{Li}_{0.38}\text{Sr}_{0.44}\text{Ta}_{0.75-x}\text{Hf}_{0.25+x}\text{O}_{3-x}\text{F}_x$ (Table S1 and Figure S1 b) increases with x because the ionic radius of Hf^{4+} is larger than that of Ta^{5+} . The $\text{Li}_{0.38}\text{Sr}_{0.44}\text{Ta}_{0.7}\text{Hf}_{0.3}\text{O}_{2.95}\text{F}_{0.05}$ (LSTHF₅) pellet has the highest density of 6.8 g cm^{-3} (Table S1), and a few closed pores were observed in the pellet (Figure S2). The density and mechanical strength of LSTHF₅ pellets were further improved by firing the LSTHF₅ powders with spark plasma sintering (SPS). The strong bonding between the grains of LSTHF₅ is evidenced by the transcrystalline rupture (Figure 1c), which increases the Li-ion transport across the grain-boundary. The LSTHF₅ pellets fired by conventional sintering and by SPS have room-temperature Li-ion conductivities of 3.3 and $4.8 \times 10^{-4} \text{ S cm}^{-1}$, respectively (Figure 1b and Figure S1 c).

High-resolution ^6Li NMR spectroscopy was performed to resolve the lithium local structural environment. The Li^+ ions in LSTHF₅ have two different local environments with resonances at $\delta = 2.49$ and 1.37 ppm (Figure 1d). The major component at $\delta = 2.49 \text{ ppm}$ corresponds to 96% of the total integral while the minor component accounts for the remaining 4%. The A site coordinated by twelve oxygen atoms in a cubic perovskite structure (ABO_3) is too large for a small Li^+ ion, and the face of the cubic framework containing four coplanar oxygen atoms is large enough to accept a Li^+ ion. The Li^+ ions in LSTHF₅ can 1) occupy the faces bordering two empty A sites (Figure S3) or 2) it is displaced from a face by electrostatic repulsion from a Sr^{2+} ion on one side of the face. The Li^+ /cubic face ratio in LSTHF₅ is close to 1:8, and the

[*] Y. Li, H. Xu, N. Wu, S. Xin, L. Xue, K. Park, J. B. Goodenough
 Materials Science and Engineering Program and Texas Materials
 Institute, University of Texas at Austin
 Austin, TX 78712 (USA)
 E-mail: jgoodenough@mail.utexas.edu

P. Chien, Y.-Y. Hu
 Department of Chemistry and Biochemistry
 Florida State University
 Tallahassee, FL 32310 (USA)

Y.-Y. Hu
 National High Magnetic Field Laboratory
 1800 East Paul Dirac Drive, Tallahassee, FL 32310 (USA)

 Supporting information and the ORCID identification number(s) for the author(s) of this article can be found under:
 <https://doi.org/10.1002/anie.201804114>

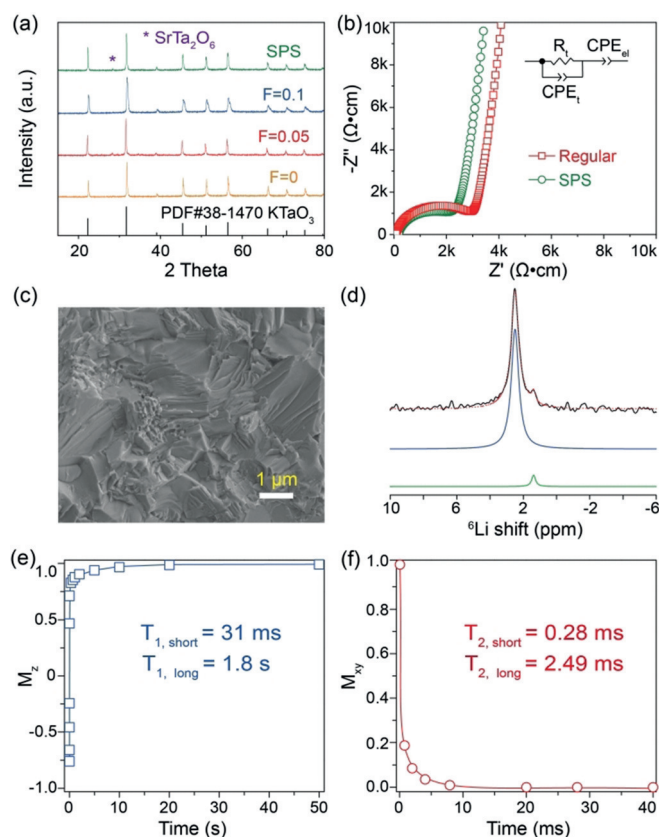


Figure 1. a) XRD patterns of $\text{Li}_{0.38}\text{Sr}_{0.44}\text{Ta}_{0.75-x}\text{Hf}_{0.25+x}\text{O}_{3-x}\text{F}_x$. b) Room-temperature electrochemical impedance plots of the LSTHF₅ pellets; the impedance plot was fitted with an equivalent circuit ($R_1\text{CPE}_1$)-(CPE_2). c) SEM image of LSTHF₅ prepared by SPS. d) High-resolution ⁶Li MAS NMR spectra of LSTHF₅; results of spectral simulations (green and blue lines and red dotted line) are displayed with the experimental spectrum (black line). e, f) ⁷Li spin-lattice relaxation times (T_1) and spin-spin relaxation times (T_2) of LSTHF₅. Both short and long T_1 and T_2 relaxation times are given in the Figure.

small activation energy of 0.3 eV was ascribed to fast Li-ion hopping between faces separating empty A sites (Figure S1d). Fast-ion dynamics are closely related to the spin-lattice (T_1) and spin-spin relaxation times (T_2). Shorter relaxation times, especially T_1 , imply fast Li-ion movement (Figure 1 e, f). The calculated T_1 and T_2 relaxation times show distinct Li-ion motion between two different sites. Most Li ions (at $\delta = 2.49$ ppm) in LSTHF₅ are more mobile as is indicated by the much shorter T_1 and T_2 times. The ratio between the two separate magnetization quantities in both T_1 and T_2 relaxation measurements agrees well with the proportion of the integrals extracted from the ⁶Li spectrum.

The electrochemical stability of LSTHF₅ tested in a Li/LSTHF₅/Au cell is shown in Figure S4; the metallic lithium anode and LSTHF₅ electrolyte were separated by a 100 μm -thick crosslinked Li-ion conductive polymer (CPEO) with a Li ion conductivity of approximately 10^{-4} Scm^{-1} at 65 °C and a high melting point exceeding 200 °C.^[7] LSTHF₅ is stable between 1.3 and 4.5 V, but is unstable at voltages below 1.3 V because of reduction of the Ta⁵⁺ ions.^[8] A solid Li⁺-conducting lithium alloy^[9] or polymer layer^[10] is usually added

between a lithium metal anode and an oxide solid electrolyte to 1) reduce the interfacial resistance, 2) retain the Li/solid-electrolyte interface during cycling, and 3) homogenize the current density through the solid electrolyte. The impedance plot of the symmetric Li/Li cell is shown in Figure 2a;

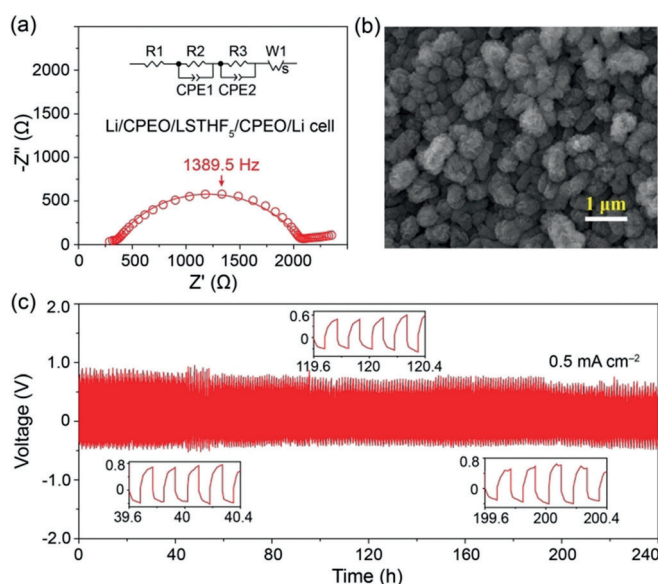


Figure 2. a) Electrochemical impedance plot of LSTHF₅ in symmetric Li electrodes at 65 °C. b) SEM image of Li metal after cycling the symmetric Li/LSTHF₅/Li cell. c) Charge and discharge voltage profiles of the Li/LSTHF₅/Li cell at 65 °C.

LSTHF₅ has a small interfacial resistance of about 220 $\Omega \text{ cm}^2$ with the CPEO, which is much smaller than that of the Li₇La₃Zr₂O₁₂ garnet electrolyte (900 $\Omega \text{ cm}^2$).^[10b] The symmetric cell cycling at 0.5 mA cm⁻² in Figure 2c has a low overpotential of 0.6 V, and there is no notable voltage increase after 240 h. Lithium only grows at the Li/CPEO interface in the form of particles with an average size of 1 μm (Figure 2b), and no lithium dendrites were observed on the Li metal surface. The symmetric Li/CPEO/Li cell was short-circuited at 0.4 mA cm⁻² after 72 h, and the voltage kept increasing, indicating an unstable interface (Figure S5). The current density of the symmetric Li/Li cell with the LSTHF₅ pellet is almost double the critical current density of the cell with a garnet electrolyte (300 $\mu\text{A cm}^{-2}$).^[6]

The chemical stability of a solid electrolyte upon exposure to moisture and CO₂ in the air determines the total internal resistance of a Li-ion battery. The exchange of electrolyte Li⁺ and the H⁺ of adsorbed water as OH⁻ and (HCO₃)⁻ occurs where the Li⁺ ions of the electrolyte are destabilized by Li⁺-Li⁺ repulsion across a shared site face, which occurs in the garnet Li₇La₃Zr₂O₁₂; the resulting LiOH and Li₂CO₃ phases on the surface and the grain boundaries of a polycrystalline membrane introduce a large internal resistance unless removed by appropriate high-temperature annealing. The mobile Li⁺ ions of the oxoperovskite LSTHF₅ do not share a common site face, and the Li⁺ ions displaced by a Sr²⁺ neighbor are not mobile. The TGA result of LSTHF₅ aged in the air for one year (LSTHF₅/1Y) in Figure S6a shows that it

has good chemical stability in the air; the weight loss of 0.1–0.15 wt % between 180 and 320 °C can be assigned to the loss of adsorbed water. The bands at 598 and 892 cm^{-1} in the Raman spectra (Figure S6b) of LSTHF₅ and LSTHF₅/1Y originate from the vibration of Hf–O and Ta–O bonds, respectively; no band at 1090 cm^{-1} corresponding to the vibration of CO_3^{2-} was observed in the Raman spectra. The fresh LSTHF₅ and LSTHF₅/1Y pellets have the same lattice parameters (4.000 Å) and nearly room-temperature Li-ion conductivity (Figure S6c,d); all results indicate the excellent stability of LSTHF₅ in the air.

The stability of an oxide solid electrolyte in water is important if it is used in an aqueous solution. However, most oxide electrolytes are unstable in water, which limits their application in an aqueous redox-flow battery.^[11] For example, the pH of neutral water increases to 12 after putting the garnet electrolyte $\text{Li}_7\text{La}_3\text{Zr}_2\text{O}_{12}$ in water for several minutes because of the fast exchange of Li^+/H^+ , and the Li-ion conductivity decreases by two orders of magnitude after the reaction. To check the structural and chemical stability of LSTHF₅ in water with different pH values, LSTHF₅ pellets were immersed in water with pH 0, 3, 7, or 14 (LSTHF₅-pH-*x*) for two weeks. The Raman spectra and XRD results of the LSTHF₅-pH-*x* ($3 \leq x \leq 14$) pellets in Figure 3a,b are the same as those of the fresh LSTHF₅ pellet, which confirms the good stability of LSTHF₅ in aqueous solution. Moreover, all of the LSTHF₅-pH-*x* ($3 \leq x \leq 14$) and fresh LSTHF₅ pellets have the same lattice parameters of 4.000 Å. The TEM images of LSTHF₅-pH-*x* ($3 \leq x \leq 14$) powders in Figure S7 show that the surfaces of the LSTHF₅ powders retained the cubic perovskite structure of the fresh LSTHF₅ sample. The room-temperature impedance plots of LSTHF₅-pH-*x* ($3 \leq x \leq 14$) pellets dried at 100 °C showed that there was no obvious change in the Li-ion conductivities between fresh LSTHF₅

and LSTHF₅-pH-*x* ($3 \leq x \leq 14$) pellets (Figure S8). The Li-ion conductivity of the LSTHF₅-pH-0 pellet decreased from 3.6×10^{-4} to $2 \times 10^{-4} \text{ S cm}^{-1}$, indicating good stability of LSTHF₅ even in a strongly acidic environment. To check the possible H^+ -ion conduction inside the perovskite after putting it in water for 14 days, Li/organic electrolyte/LSTHF₅-pH-*x*/organic electrolyte/LiFePO₄ batteries with LSTHF₅-pH-*x* pellets dried at 100 °C as separators were prepared; the Li/LiFePO₄ battery had a total resistance of approximately 400 Ω (Figure S9a). The small overpotential and good cycling performance of a Li/LiFePO₄ battery (Figure S9b,c) indicate that the conductivity of the LSTHF₅-pH-*x* ($3 \leq x \leq 14$) pellets is due to Li-ion transport and not to H-ion transport.

To further check the electrochemical stability of LSTHF₅ in water with different pH values, a symmetric C/LSTHF₅/C supercapacitor with LSTHF₅ as the separator was tested; aqueous electrolytes with different pH values were added into the carbon electrodes. In Figure S10, the LSTHF₅ had an interfacial resistance of 165 Ω cm^2 with carbon electrodes wet by the electrolyte. The charge/discharge curves of the supercapacitors with $3 \leq \text{pH} \leq 14$ in Figure 3c show a symmetric triangular shape from the electric-double-layer capacitance, and the specific capacitances are about 70–80 F g^{-1} . The cycling capability of the C/LSTHF₅/C supercapacitors at 0.1 mA cm^{-2} in Figure 3d showed that the specific capacitance of C/LSTHF₅/C at pH 3, 7, and 14 retained, respectively, over 95, 93, and 92.5% of its initial value after 1000 cycles (Figure 3d), which indicates that the LSTHF₅ is electrochemically stable in aqueous solution with $3 \leq \text{pH} \leq 14$.

The excellent stability of LSTHF₅ in moist air and in aqueous solution helps to reduce the interfacial resistance of a Li-ion battery. An all-solid-state Li/LiFePO₄ battery with the LSTHF₅ electrolyte was assembled to check the Li-ion transport across the LSTHF₅ interfaces. The Li-metal anode and the LSTHF₅ pellet were separated by the CPEO polymer, which can suppress lithium-dendrite formation at the Li-metal/polymer interface as confirmed in the symmetric Li/Li cell. Carbon and the CPEO were added into the LiFePO₄ cathode to provide electronic and ionic conductivities. In Figure S11a, the total resistance of the all-solid-state Li/LiFePO₄ battery at 65 °C is about 600 Ω cm^2 , which is much smaller than that of the reported all-solid-state battery with a fast Li-ion-conducting garnet pellet.^[10b] LSTHF₅ shows a small interfacial resistance of 380 Ω cm^2 with the composite LiFePO₄ cathode. The LSTHF₅ electrolyte also shows a much smaller interfacial resistance with the solid polymer and the composite LiFePO₄ cathode than the antiperovskite $\text{Li}_2(\text{OH})_{0.9}\text{F}_{0.1}\text{Cl}$ electrolyte because the antiperovskite electrolyte is highly unstable even in an organic electrolyte.^[5c,10a] The all-solid-state Li/LiFePO₄ cell had low overpotentials of 0.15 and 0.28 V at 150 and 300 $\mu\text{A cm}^{-2}$, respectively, with corresponding initial discharge capacities of 142 and 128 mAh g^{-1} (Figure 4a). Capacities of 120 and 82 mAh g^{-1} at 150 and 300 $\mu\text{A cm}^{-2}$ were retained after 100 and 200 cycles with a high coulombic efficiency of 99.8–100% (Figure 4b).

To study the interfacial resistance and the performance of LSTHF₅ in a Li redox-flow battery, a Li-S cell with the LSTHF₅ solid electrolyte was assembled. The garnet and LISICON electrolytes have been shown in hybrid Li-S

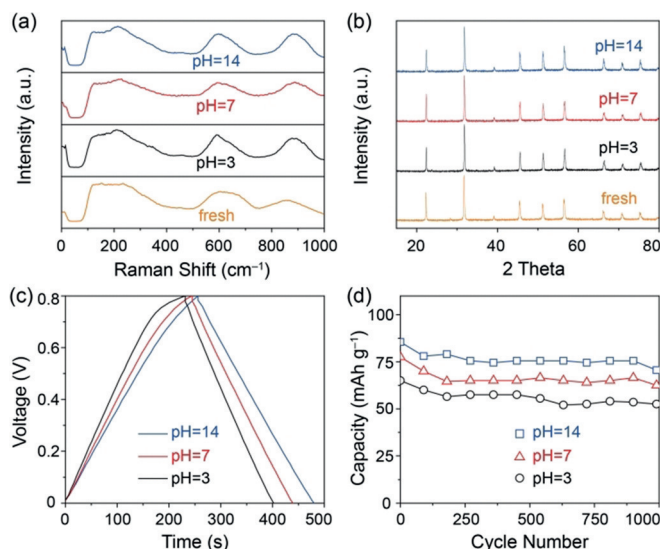


Figure 3. The chemical and electrochemical stability of LSTHF₅ in water with different pH values. a) Raman spectra, b) XRD patterns, c) charge/discharge curves, and d) the cycling performance of C/LSTHF₅/C supercapacitors with LSTHF₅ treated with water of different pH values.

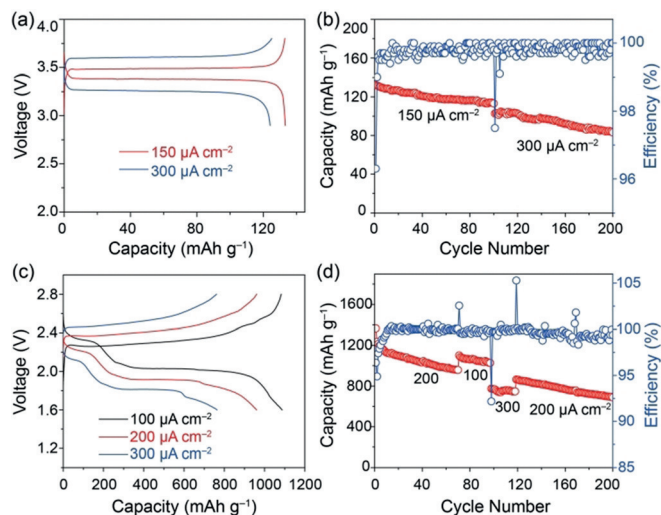


Figure 4. All-solid-state Li-metal battery operating at 65 °C. a) Charge/discharge voltage profiles at 150 and 300 $\mu\text{A cm}^{-2}$. b) Capacity retention and cycling efficiency. Electrochemical characterization of a Li-S battery operating at 25 °C. c) Charge/discharge curves. d) The cycling performance at different current densities.

batteries to block the severe polysulfide shuttle problem, but the garnet electrolyte had a large interfacial resistance ($2620 \Omega \text{ cm}^2$) with an inorganic electrolyte while the LISICON $\text{Li}_{1.3}\text{Al}_{0.3}\text{Ti}_{1.7}(\text{PO}_4)_3$ electrolyte reacted with the polysulfide anions.^[10b,12] The LSTHF₅ electrolyte is stable in a Li-S battery because of the relatively large electrochemical window. The total resistance of the Li-S cell with LSTHF₅ in Figure S11b was $800 \Omega \text{ cm}^2$, which is one third of that of the Li-S cell with the garnet electrolyte.^[10b] LSTHF₅ displayed a smaller interfacial resistance than LSHTF_x with $x = 0$ in the Li-S and all-solid-state Li/LiFePO₄ cell (Figure S11); the residual LiF on the grain surface may increase the stability of the perovskite. The Li-S cell featured a small discharge versus charge voltage gap (0.34 and 0.45 V) and discharge capacities of 1074 and 980 mAh g^{-1} at 100 and 200 $\mu\text{A cm}^{-2}$, respectively (Figure 4c). The cell has a high coulombic efficiency of almost 100% over the subsequent 200 cycles (Figure 4d), which is much higher than that of the Li-S cell without LSTHF₅, indicating that the LSTHF₅ can efficiently block the polysulfide shuttle. The reversible cycling capacities stabilized at about 975 mAh g^{-1} after 100 cycles with retention of 90.7% of the stabilized capacity in the second cycle. After cycling the Li-S battery, the LSTHF₅ pellet gave rise to the same Raman spectrum and XRD pattern as the fresh LSTHF pellet (Figure S12), indicating excellent stability of LSTHF₅ in Li-S batteries.

The chemical stability of oxide Li-ion electrolytes has a great influence on the Li-ion transport across the electrode/electrolyte interfaces in an all-solid-state Li-ion battery and a Li-redox-flow battery. The new oxoperovskite electrolyte $\text{Li}_{0.38}\text{Sr}_{0.44}\text{Ta}_{0.7}\text{Hf}_{0.3}\text{O}_{2.95}\text{F}_{0.05}$ (LSTHF₅) has a high room-temperature Li-ion conductivity of $4.8 \times 10^{-4} \text{ S cm}^{-1}$ and good electrochemical stability up to 4.5 V. This perovskite electrolyte, which is stable in aqueous solution with pH 3–14, has a much smaller interfacial resistance in aqueous solution,

a solid composite cathode, and a commercial organic electrolyte. The all-solid-state Li/LiFePO₄ battery and a hybrid Li-S battery with LSTHF₅ solid electrolytes have high coulombic efficiencies of 99.7–100% with stable long-term cycling performances.

Acknowledgements

This work was supported by the Assistant Secretary for Energy Efficiency and Renewable Energy, Office of Vehicle Technologies of the U.S. Department of Energy through the Advanced Battery Materials Research (BMR) Program award number 7223523 and Battery500 Consortium award number DE-EE0007762.

Conflict of interest

The authors declare no conflict of interest.

Keywords: all-solid-state batteries · electrolytes · hybrid Li-S batteries · interfacial resistance · perovskites

How to cite: *Angew. Chem. Int. Ed.* **2018**, *57*, 8587–8591
Angew. Chem. **2018**, *130*, 8723–8727

- [1] a) J. B. Goodenough, Y. Kim, *Chem. Mater.* **2010**, *22*, 587–603; b) A. Manthiram, X. Yu, S. Wang, *Nat. Rev. Mater.* **2017**, *2*, 16103; c) Y. Kato, S. Hori, T. Saito, K. Suzuki, M. Hirayama, A. Mitsui, M. Yonemura, H. Iba, R. Kanno, *Nat. Energy* **2016**, *1*, 16030.
- [2] a) Y. Li, W. Zhou, X. Chen, X. Lü, Z. Cui, S. Xin, L. Xue, Q. Jia, J. B. Goodenough, *Proc. Natl. Acad. Sci. USA* **2016**, *113*, 13313–13317; b) Q. Pang, X. Liang, A. Shyamsunder, L. F. Nazar, *Joule* **2017**, *1*, 871–886.
- [3] J. B. Goodenough, *Nat. Electron.* **2018**, *1*, 204–204.
- [4] a) H. Duan, Y.-X. Yin, Y. Shi, P.-F. Wang, X.-D. Zhang, C.-P. Yang, J.-L. Shi, R. Wen, Y.-G. Guo, L.-J. Wan, *J. Am. Chem. Soc.* **2018**, *140*, 82–85; b) X. Zhang, T. Liu, S. Zhang, X. Huang, B. Xu, Y. Lin, B. Xu, L. Li, C.-W. Nan, Y. Shen, *J. Am. Chem. Soc.* **2017**, *139*, 13779–13785.
- [5] a) L. Cheng, E. J. Crumlin, W. Chen, R. Qiao, H. Hou, S. Franz Lux, V. Zorba, R. Russo, R. Kostecki, Z. Liu, K. Persson, W. Yang, J. Cabana, T. Richardson, G. Chen, M. Doeff, *Phys. Chem. Chem. Phys.* **2014**, *16*, 18294–18300; b) S. D. Jackman, R. A. Cutler, *J. Power Sources* **2013**, *230*, 251–260; c) D. J. Schroeder, A. A. Hubaud, J. T. Vaughney, *Mater. Res. Bull.* **2014**, *49*, 614–617; d) L. Truong, M. Howard, O. Clemens, K. S. Knight, P. R. Slater, V. Thangadurai, *J. Mater. Chem. A* **2013**, *1*, 13469–13475.
- [6] A. Sharafi, E. Kazyak, A. L. Davis, S. Yu, T. Thompson, D. J. Siegel, N. P. Dasgupta, J. Sakamoto, *Chem. Mater.* **2017**, *29*, 7961–7968.
- [7] W. Zhou, S. Wang, Y. Li, S. Xin, A. Manthiram, J. B. Goodenough, *J. Am. Chem. Soc.* **2016**, *138*, 9385–9388.
- [8] B. Huang, B. Xu, Y. Li, W. Zhou, Y. You, S. Zhong, C.-A. Wang, J. B. Goodenough, *ACS Appl. Mater. Interfaces* **2016**, *8*, 14552–14557.
- [9] a) K. Fu, Y. Gong, B. Liu, Y. Zhu, S. Xu, Y. Yao, W. Luo, C. Wang, S. D. Lacey, J. Dai, Y. Chen, Y. Mo, E. Wachsman, L. Hu, *Sci. Adv.* **2017**, *3*, e1601659; b) W. Luo, Y. Gong, Y. Zhu, K. K. Fu, J. Dai, S. D. Lacey, C. Wang, B. Liu, X. Han, Y. Mo, E. D. Wachsman, L. Hu, *J. Am. Chem. Soc.* **2016**, *138*, 12258–12262;

- c) X. Han, Y. Gong, K. Fu, X. He, G. T. Hitz, J. Dai, A. Pearce, B. Liu, H. Wang, G. Rubloff, Y. Mo, V. Thangadurai, E. D. Wachsman, L. Hu, *Nat. Mater.* **2016**, *16*, 572.
- [10] a) Y. Li, W. Zhou, S. Xin, S. Li, J. Zhu, X. Lü, Z. Cui, Q. Jia, J. Zhou, Y. Zhao, J. B. Goodenough, *Angew. Chem. Int. Ed.* **2016**, *55*, 9965–9968; *Angew. Chem.* **2016**, *128*, 10119–10122; b) Y. Li, B. Xu, H. Xu, H. Duan, X. Lü, S. Xin, W. Zhou, L. Xue, G. Fu, A. Manthiram, J. B. Goodenough, *Angew. Chem. Int. Ed.* **2017**, *56*, 753–756; *Angew. Chem.* **2017**, *129*, 771–774.
- [11] Y. Zhao, Y. Ding, Y. Li, L. Peng, H. R. Byon, J. B. Goodenough, G. Yu, *Chem. Soc. Rev.* **2015**, *44*, 7968–7996.
- [12] X. Yu, Z. Bi, F. Zhao, A. Manthiram, *Adv. Energy Mater.* **2016**, *6*, 1601392.

Manuscript received: April 6, 2018

Accepted manuscript online: May 7, 2018

Version of record online: June 7, 2018